Theoretical Determination of Transfer Length in Pretensioned Members Using Thick Cylinder Theory

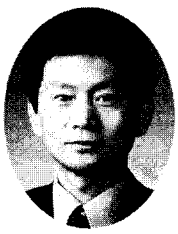

Oh, Byung-Hwan* Kim, Eui-Sung**

Abstract

The extensive usage of pretensioned prestressed concrete component in modern construction as structural members mandates precise understanding of its mechanism. Especially, an adequate transfer of prestressing force from steel tendons to concrete around the end regions of the member is a critical issue. Due to the importance of the topic, several investigators have formulated equations modeling the transfer bond length based on various bonding mechanism between steel and concrete. However, the existing models are still inadequate in predicting the bond development in pretensioned prestressed concrete members. Therefore, this study presents a model of transfer bond length based on rational theory that can simulate experimental results. The model is developed into solid mechanics based structural analysis computer program. The program is validated by comparing the analysis results with experimental results of bond stress distribution, concrete strain profiles, and transfer length in pretensioned prestressed concrete members. The proposed analytical procedure in this study can be utilized as a useful tool for realistic evaluation of transfer length in pretensioned prestressed concrete members.

Keywords : pretensioned prestressed concrete, transfer of prestress forcce, bond stress distribution, concrete strain profile, transfer length

* KCI Member, Professor, Department of Civil Engineering, Seoul National University, Korea
** KCI Member, Researcher, Civil Division, Hyundai Development Company, Seoul, Korea

1. Introduction

The extensive use of prestressed concrete in the modern construction industry, together with wider application of pretensioned components for structural purposes requires some important consideration on the adequate transfer of prestress force into the concrete, especially around the end zones of pretensioned member.

In response to this need for research, several investigators have formulated equations for transfer bond length based on different concepts of bond between steel and concrete.[1-7] However, these theories formulated for transfer bond have been neither convincing nor successful in predicting bond development. Therefore, it was considered important to formulate a rational theoretical basis. Moreover, during the analysis of the test data, the search for solutions to the prestress transfer problem was motivated by the absence of valid theory to complement experiments.

In this paper, a detailed procedure based on the principles of solid mechanics has been presented and validated by comparison with relevant experimental results in order to determine the transfer length.

2. Bond Mechanism

Bond in general can be defined as the property, which causes hardened concrete to grip an embedded steel in such a manner as to resist forces of the tendon tending to slide longitudinally through the concrete. The bond stress, τ can be generally expressed by the following equation.

$$\tau = \mu p \tag{1}$$

The coefficient μ can be considered constant for a particular type of steel and combines actual frictional bond and the mechanical bond resulting from deformations projecting from the tendon surface. The interface characteristics of the tendon determine the relative proportions of the mechanical and the frictional components in the bond mechanism. The overall friction coefficient, μ, can be determined experimentally. If the coefficient of friction is known experimentally,[8,9] the bond stress can be found if the interface pressure, p (value of radial stress), can be determined. To determine the unknown quantity p, a general procedure is developed using the theory of elasticity applied to thick-walled cylinders.[10]

3. Isotropic Elastic Analysis

To make an analysis possible, it is necessary to make some simplifying assumptions. A typical idealization of the anchorage zone for a hollow core slab and a rectangular beam is illustrated in Fig. 1.

Steel is treated as a solid cylinder and concrete as a hollow cylinder with a radius equal to the smaller cover c_s.[8,11] The outer surface of the notional concrete cylinder is assumed to behave as a free surface. The physical dimensions are shown in Fig. 2.

The radius of the steel cylinder is equal to r_o (the radius of the unstressed steel). The concrete cylinder has an outer radius of c and an inner radius of r_j which is the radius of the stressed steel because the concrete is cast when the tendon is in its stressed state. At transfer of the prestressing force, steel shortens and swells so a pressure p develops at the interface. Using thick cylinder theory,[10] expressions for displacements and stresses of the element can be developed by ensuring equilibrium and compatibility, and imposing boundary conditions and constitutive relationships that properly represent the material behavior.

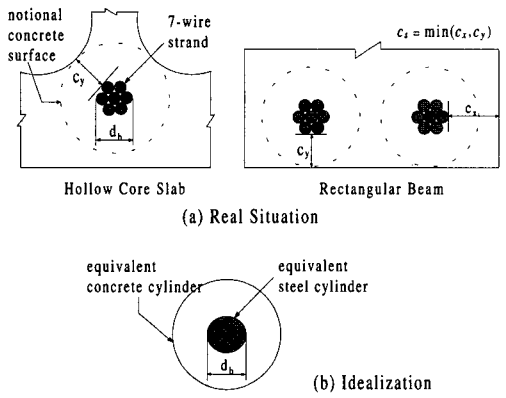

Fig. 1 Real situations and idealization

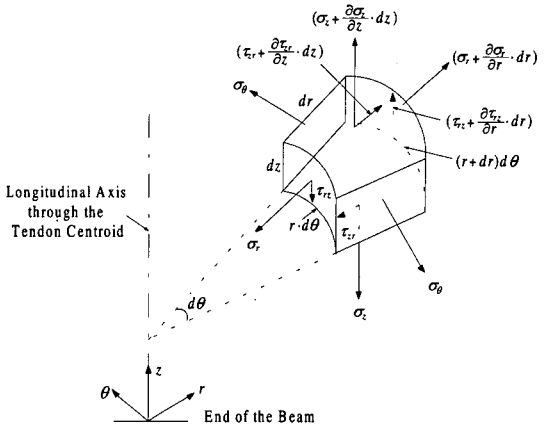

Fig. 3 Three dimensional stresses acting on element

3.1 Equilibrium Equation

An element in the form of a slice of thickness dz is taken at a distance z from the end to derive an equilibrium equation [refer to Fig. 3]. Three-dimensional equilibrium of forces in the radial direction can be solved by dropping terms containing higher-order infinitesimal.[10]

$$\sigma_r + \frac{\partial \sigma_r}{\partial r} \cdot r - \sigma_\theta + \frac{\partial \tau_{zr}}{\partial z} \cdot r = 0 \qquad (2)$$

In the longitudinal direction, all the variables are assumed to be independent of z direction within the finite length dz. Therefore, Eq. (2) is reduced to Eq. (3).

$$\sigma_r + \frac{d\sigma_r}{dr} \cdot r - \sigma_\theta = 0 \qquad (3)$$

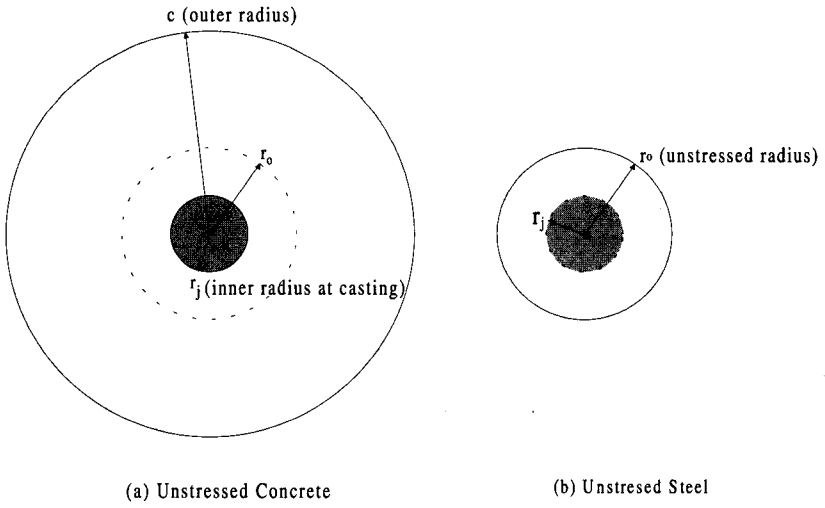

Fig. 2 Physical dimensions of steel and concrete cylinder

3.2 Compatibility Condition

The basic requirement to be fulfilled is the compatibility of displacements at the steel-concrete interface given by following equation (see Fig. 4).[11]

$$r_o + u_o = u_j + r_j \tag{4}$$

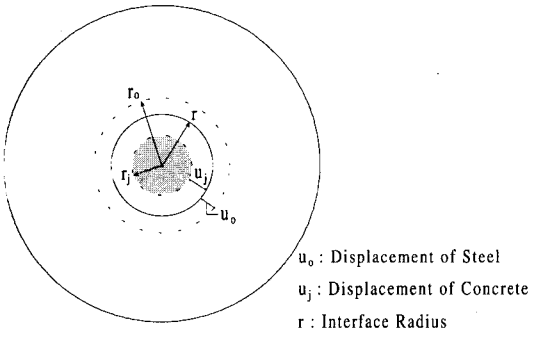

Fig. 4 Relative radial displacement of stressed composite unit

3.3 Derivation of Circumferential and Radial Stresses

From strain-displacement and stress-strain relations of the element, stresses in radial and circumferential direction are derived as Eq. (5).

$$\begin{aligned}\sigma_r &= \frac{E}{1-v^2}(\varepsilon_r + v\varepsilon_\theta) + \frac{v(1+v)\sigma_z}{1-v^2} \\ \sigma_\theta &= \frac{E}{1-v^2}(\varepsilon_\theta + v\varepsilon_r) + \frac{v(1+v)\sigma_z}{1-v^2}\end{aligned} \tag{5}$$

Substituting Eq. (5) into Eq. (3) results in the following equidimensional equation in radial displacement (u).

$$r\frac{d^2u}{dr^2} + \frac{du}{dr} - \frac{u}{r} = 0 \tag{6}$$

This equation is solved by u as

$$u = c_1 r + \frac{c_2}{r} \tag{7}$$

The radial and circumferential stresses may now be written in terms of the constants of integration c_1 and c_2 by combining Eqs. (7) & (5).

$$\begin{aligned}\sigma_r &= E\left\{\frac{c_1}{(1-v)} - \frac{c_2}{r^2(1+v)}\right\} + \frac{v\sigma_z}{(1-v)} \\ \sigma_\theta &= E\left\{\frac{c_1}{(1-v)} + \frac{c_2}{r^2(1+v)}\right\} + \frac{v\sigma_z}{(1-v)}\end{aligned} \tag{8}$$

The constant c_1 and c_2 can be determined using the boundary conditions. For solution purpose, two cases with different boundary conditions were considered and expressions for $\sigma_r, \sigma_\theta, u$ were derived for each case.

(a) Case - Solid Steel Cylinder

Boundary condition of the solid cylinder is $u = 0$ at $r = 0$. Therefore the constant c_2 of Eq. (7) must be zero. So Eq. (8) is written as

$$\sigma_r = \sigma_\theta = \frac{(Ec_1 + v\sigma_z)}{(1-v)}$$

This equation is independent of r. Therefore suppose that $\sigma_r = \sigma_\theta = f_r$ at $r = R$, then we have the following expression for displacement.

$$u = \left[\frac{f_r(1-v) - v\sigma_z}{E}\right] r \tag{9}$$

(b) Case - Hollow Concrete Cylinder

Boundary conditions of the hollow cylinder are $\sigma_r = f_r$ at $r = R$ and $\sigma_r = 0$ at $r = c$. From these boundary conditions, following expressions for $\sigma_r, \sigma_\theta, u$ are obtained.

$$\sigma_r = \frac{f_r(1/c^2 - 1/r^2)}{(1/c^2 - 1/R^2)}$$
$$\sigma_\theta = \frac{f_r(1/c^2 + 1/r^2)}{(1/c^2 - 1/R^2)} \quad (10)$$

$$u = \frac{f_r r}{E(1/c^2 - 1/R^2)}\left[\frac{(1-\nu)}{c^2} + \frac{(1+\nu)}{r^2}\right] - \frac{\nu\sigma_z r}{E} \quad (11)$$

Based on the results of above two cases, an expression for the interface pressure can be obtained. For the solid steel cylinder, the displacement at its outer surface can be written from Eq. (9) as

$$u_o = \left[\frac{-p(1-\nu_p) - \nu_p f_{pz}}{E_p}\right] r_o \quad (12)$$

For the concrete cylinder, the displacement at its inner surface is given by Eq. (11) as

$$u_j = \frac{-pr_j}{E_c(1/c^2 - 1/r_j^2)}\left[\frac{(1-\nu_c)}{c^2} + \frac{(1+\nu_c)}{r_j^2}\right] - \frac{\nu_c f_{cz} r_j}{E_c} \quad (13)$$

From the compatibility condition, an expression for the interface pressure is obtained.

$$p = \frac{r_o(1-\nu_p f_{pz}/E_p) - r_j(1-\nu_c f_{cz}/E_c)}{(1-\nu_p)r_o/E_p + [\nu_c - (r_j^2 + c^2)/(r_j^2 - c^2)]r_j/E_c} \quad (14)$$

Finally, the radial and circumferential stresses, σ_r and σ_θ, can be expressed as follows.

$$\sigma_r = \frac{-p(1/c^2 - 1/r^2)}{(1/c^2 - 1/R^2)}$$
$$\sigma_\theta = \frac{-p(1/c^2 + 1/r^2)}{(1/c^2 - 1/R^2)} \quad (15)$$

3.4 Transverse Stress Distribution

To demonstrate the stress distribution a numerical example is considered. For a tendon diameter d_b = 12.7mm, effective prestress f_{pe} = 1300MPa, clear cover c_s = 30mm and concrete strength at transfer f_{ci}= 30MPa, the radial and circumferential stress distributions for a slice taken at the free end are shown in Fig. 5.

The analysis shows that tensile stress in the circumferential direction attains values approximately 10 times the concrete tensile strength. It is therefore clear that the concrete must crack in the radial direction to accommodate the swelling of the released tendon. This cracking will alter the stiffness of the concrete in the damaged region around the tendon. This simple analysis shows that concrete cannot be treated as an isotropic material.

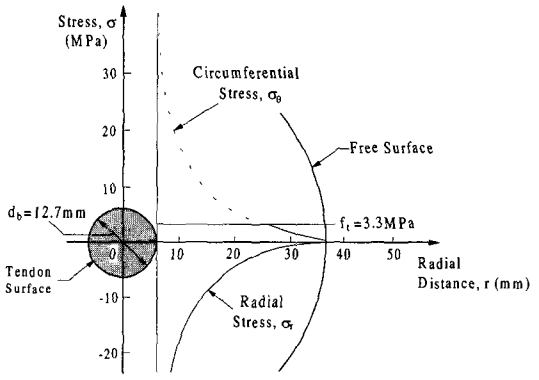

Fig. 5 Transverse stress distributions from isotropic elastic analysis

4. Characteristics of Radially Cracked Concrete

4.1 Nature of Fractured Zone

It is instructive to examine a region around the tendon as illustrated in Fig. 6.[11] This situation

was suggested based on the characteristics of damaged region in reinforced concrete beam presented by Hillerborg.[12] The length of the damaged zone (L_c) is defined as the distance measured from the effective crack tip to the surface of the steel.

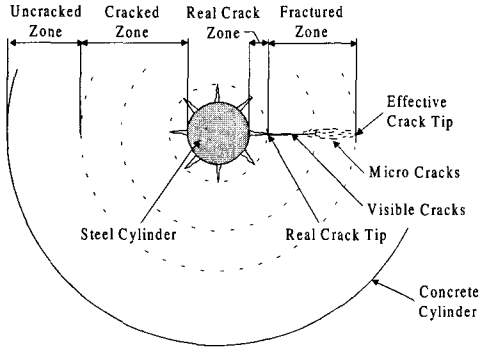

Fig. 6 Nature of cracking around tendon

4.2 Modeling of Fractured Concrete

To represent the degree of cracking, two parameters, the reduced maximum tensile strength (f_{tr}) and the length of damaged zone (L_c) are important. Three possible situations need to be considered as shown in Fig. 7. When a tendon is released, the concrete near the end of the tendon may become fully cracked.

The concrete surrounding the tendon will be only partially cracked where the reduction of stress in the steel is small while the concrete near the end of the transfer zone is uncracked.

When cracking occurs in the radial direction, an anisotropic analysis with the circumferential (θ) direction is required. One of the primary effects of radial cracking is to reduce the stiffness in the circumferential direction. This is accounted for by using a reduced modulus of elasticity $E_\theta < E_c$ in the circumferential direction. The solution used to determine the stresses for the 3-cases can be summarized as:

Case	Conc. Cylinder	Type of Analysis
I	Uncracked	Isotropic
II	Partly Cracked	Outer Cylinder-Isotropic
		Inner Cylinder-Anisotropic
III	Fully Cracked	Anisotropic

The influence of cracking is determined by relating this phenomenon to the softening behavior of concrete in tension.

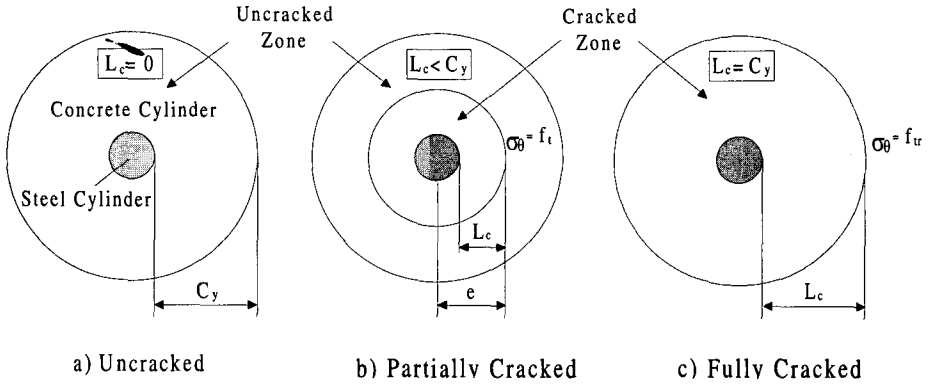

Fig. 7 Possible situations for analysis

4.3 Behavior of Concrete in Tension

In the anchorage problem, the cracking that occurs can be related to the uniaxial tension tests but the cracks radiating from the bar have a variable width and spacing. With increasing radial distance, the crack width reduces while crack spacing increases. Based on the test data presented by Gopalaratnam and Shâh,[14] a rectangular hyperbola of the form given by

$$(\sigma_\theta + h)(w + k) = m \tag{16}$$

is assumed[11] as shown in Fig. 8.

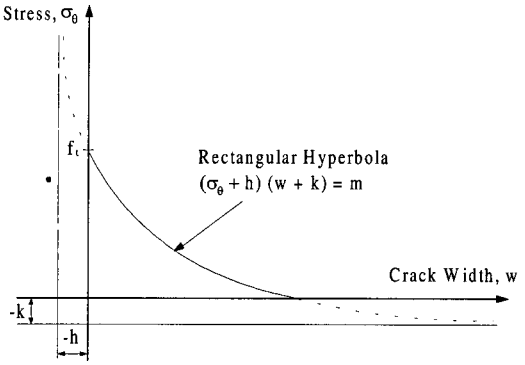

Fig. 8 Assumed stress-crack width curve for concrete in tension

5. Adjusted Elastic Properties for Anisotropic Analysis

A reduced circumferential modulus of elasticity at the outer surface of cracked concrete (E_{cr}) and a reduced tensile strength of concrete at the outer surface (f_{tr}) are required for partially cracked and fully cracked analysis procedures.

5.1 Determination of E_θ

The strain due to σ_θ only maybe written as:

$$\varepsilon = \frac{\sigma_\theta}{E_c} + \frac{w}{L} = \frac{\sigma_\theta}{E_c} + \frac{wN}{2\pi r} \tag{17}$$

By definition for a uniaxial condition,

$$E_\theta = \frac{\sigma_\theta}{\varepsilon} = \frac{\sigma_\theta}{\sigma_\theta / E_c + w/L} \tag{18}$$

which can be written using Eq. (16) as:

$$E_\theta = \frac{\sigma_\theta}{\sigma_\theta / E_c + (m/(\sigma_\theta + h) - k)N/2\pi r} \tag{19}$$

5.2 Determination of f_{tr}

The maximum reduced tensile strength may be determined from the solution (σ_θ) of the following quadratic equation.

$$\left[\frac{1}{E_c}\frac{1}{E_\theta}\right]\sigma_\theta^2 + \left[h\left(\frac{1}{E_c}\frac{1}{E_\theta}\right)\frac{kN}{2\pi r}\right]\sigma_\theta + \left[\frac{mN}{2\pi r}\frac{khN}{2\pi r}\right] = 0 \tag{20}$$

When a crack extends to the free surface $r = c$, the maximum $E_c = E_{cr}$. Then the corresponding $\sigma_\theta = f_{tr}$.

6. Anisotropic Elastic Analysis for Concrete with Radial Cracking

6.1 Governing Differential Equation

In case of anisotropic elastic analysis of the concrete with radial cracking, the constitutive relationships are different from that of the isotropic uncracked analysis. These can be written in the following form.

$$\begin{Bmatrix}\varepsilon_r \\ \varepsilon_\theta \\ \varepsilon_z\end{Bmatrix} = \frac{1}{E_c}\begin{bmatrix}1 & -\nu_c & -\nu_c \\ -\nu_c & E_c/E_\theta & -\nu_c \\ -\nu_c & -\nu_c & 1\end{bmatrix}\begin{Bmatrix}\sigma_r \\ \sigma_\theta \\ \sigma_z\end{Bmatrix} \tag{21}$$

From Eq. (21) we have

$$\sigma_r = \frac{E_c}{E_c - v_c^2 E_\theta}\left[E_c\varepsilon_r + v_c E_\theta \varepsilon_\theta\right] + \frac{v_c(E_c + v_c E_\theta)\sigma_z}{E_c - v_c^2 E_\theta}$$
$$\sigma_\theta = \frac{E_c E_\theta}{E_c - v_c^2 E_\theta}\left[v_c\varepsilon_r + \varepsilon_\theta\right] + \frac{v_c E_c(1+v_c)\sigma_z}{E_c - v_c^2 E_\theta} \quad (22)$$

Substituting Eq. (22) into Equilibrium Eq. (3) results in following 2nd order nonlinear non-homogeneous differential equation as:

$$rE_c^2\left[E_c - v_c^2 E_\theta\right]\frac{d^2u}{dr^2} + E_c^2\left[E_c + rv_c^2 E_\theta' - v_c^2 E_\theta\right]\frac{du}{dr}$$
$$+ E_c\left[rE_c v_c E_\theta' - E_\theta\left(E_c - v_c^2 E_\theta\right)\right]\frac{u}{r}$$
$$+\left[\left(E_c - v_c^2 E_\theta\right)\left(E_c - E_\theta\right) + rv_c E_c(1+v_c)E_\theta'\right]\sigma_z v_c = 0 \quad (23)$$

where E_θ' can be obtained using Eq. (24), (25) and (26) for a particular value of w.

$$\frac{dE_\theta}{dr} = \frac{N}{2\pi r}\cdot\frac{\left[-wmw'/(w+k)^2 - (m/(w+k)-h)(w'-w/r)\right]}{\left[(m/(w+k)-h)/E_c + wN/2\pi r\right]^2} \quad (24)$$

$$w' = \frac{\varepsilon' + Nw/2\pi r^2}{N/2\pi r - m/E_c(w+k)^2} \quad (25)$$

$$\varepsilon' = \frac{\sigma_r - E_c\varepsilon}{E_c r} \quad (26)$$

6.2 Numerical Solution for *U*

The numerical solution technique, Runge-Kutta method,[15] was selected to solve the differential equation. To use the fourth order Runge-Kutta method, Eq. (23) is rearranged in the following form.

$$u'' = f(u',\ u,\ r) \quad (27)$$

If initial values are u_n', u_n, r_n, then u_{n+1}', u_{n+1}, r_{n+1} at the end of step can be calculated. By repeating the procedure with $u_{n+1}', u_{n+1}, r_{n+1}$ as new initial values, the quantities at the inner radius can be found after a number of iterations.

6.3 Determination of Initial Values

To perform the analysis using the numerical method, initial values u and $u'(=du/dr)$ have to be determined using the known boundary conditions at the outer surface of the cracked cylinder. There are two possible situations depending on the extent of the damaged zone and the degree of cracking.

(a) Fully Cracked Concrete Cylinder

The known boundary conditions are $\sigma_r = 0$, $\sigma_\theta = f_{tr}$ at $r = c$ and $E_\theta = E_{cr}$ at the outer surface. Applying these boundary conditions in Eq. (21), we have initial values as

$$\left(\frac{du}{dr}\right)_c = \frac{-v_c}{E_c}\left(f_{tr} + f_{cz}\right) \quad (28)$$

$$u_c = c\left(\frac{f_{tr}}{E_{cr}} - \frac{v_c f_{cz}}{E_c}\right) \quad (29)$$

(b) Partially Cracked Concrete Cylinder

The known boundary conditions are $\sigma_r = 0$ at $r = c$ and $\sigma_\theta = f_t$ at $r = e$. Applying these boundary conditions, we have initial values as:

$$\left(\frac{du}{dr}\right)_e = \frac{1}{E_c}\left[\frac{f_t(1/c^2 - 1/e^2)}{(1/c^2 + 1/e^2)} - v_c f_t - v_c f_{cz}\right] \quad (30)$$

$$u_e = \frac{e}{E_c}\left[-v_c f_t\frac{(1/c^2 - 1/e^2)}{(1/c^2 + 1/e^2)} + f_t - v_c f_{cz}\right] \quad (31)$$

6.4 Solution Procedure

The approach of anisotropic cracked analysis is similar to the isotropic uncracked analysis except for the procedure to determine the displacement at inner surface of concrete, u_j. This displacement is obtained with the numerical solution using the Runge-Kutta method.[15]

From the initial values $(\varepsilon_r, \varepsilon_\theta)$ at the outer surface of the cracked cylinder, radial and circumferential stresses can be calculated as follows.

$$\sigma_r = E_c\varepsilon_r + v_c\sigma_\theta + v_c\sigma_z \tag{32}$$

$$\left(v_c^2-1\right)\sigma_\theta^2+\left[E_c\varepsilon_\theta+v_cE_c\varepsilon_r+v_c\sigma_z\left(1+v_c\right)+h\left(v_c^2-1\right)+\frac{NE_ck}{2\pi r}\right]\sigma_\theta$$

$$+\left\{\left[E_c\varepsilon_\theta+v_cE_c\varepsilon_r+v_c\sigma_z\left(1+v_c\right)\right]h+\frac{NE_c}{2\pi r}\left[kh-m\right]\right\}=0 \tag{33}$$

Now using Eq. (32), (19), (18), (17), (26), (25), (24), σ_r, E_θ, w, ε, ε', w', E'_θ can be determined in sequence. Therefore repeating the above procedure enables the determination of $(u)_{r_j}$, $(du/dr)_{rj}$, $(\sigma_r)_{rj}$ at inner boundary of the cracked concrete defined by $r = r_j$.

Finally, we have an expression for the interface pressure from compatibility condition.

$$p=\frac{r_o-r_j-(u)_{r_j}-r_ov_pf_{pz}/E_p}{r_o(1-v_p)/E_p} \tag{34}$$

7. Construction of Prestress Build up Curves

Once the interface pressure, p, is known, the bond stress, τ, can be determined for a particular Δz increment. The change of stress in the z direction, Δf_{pz}, may be computed from the element in Fig. 9. From the equilibrium in the longitudinal direction we have

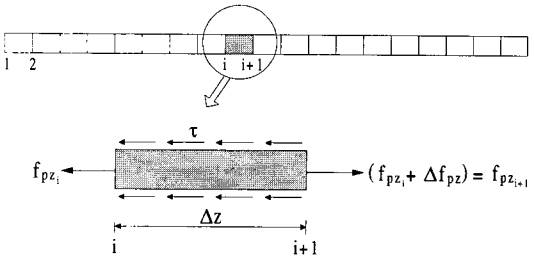

Fig. 9 Isolated steel part from the sliced element

$$\Delta f_{pz}=\frac{\pi d_b\Delta z\tau}{A_p} \tag{35}$$

Therefore the value of steel stress and prestressing force at section $i+1$ is

$$\left(f_{pz}\right)_{i+1}=\left(f_{pz}\right)_i+\Delta f_{pz} \tag{36}$$

$$P_{i+1}=\sum_{i=1}^{n}\left[\left(f_{pz}\right)_{i+1}A_p\right] \tag{37}$$

The stress in concrete at the level of the tendon under consideration is

$$\left(f_{cz}\right)_{i+1}=P_{i+1}\left[\frac{1}{A}+\frac{e_y}{I}y\right] \tag{38}$$

The step by step analysis can be carried out for increments of Δz from the free end until the steel stress reaches the effective prestress, f_{pe}, where the bond stress $\tau \cong 0$. Then the theoretical prestress build-up curves can be constructed as shown in Fig. 10 (refer to Table 1). The shape of the prestress build-up profile can have concave, linear or convex portions as shown in Fig. 11. Usually all 3-cases (namely I, II, III) appear as shown in Fig. 11. The fully cracked zone (concave portion) will not occur when the concrete stiffness is high.

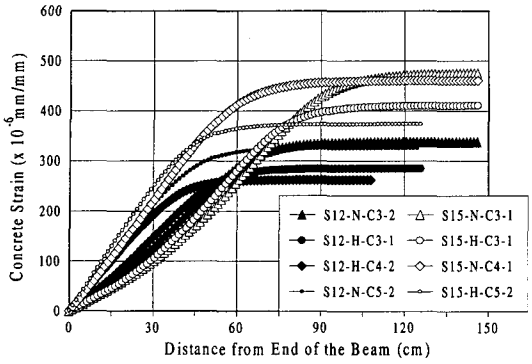

Fig. 10 Typical theoretical prestress build-up curves

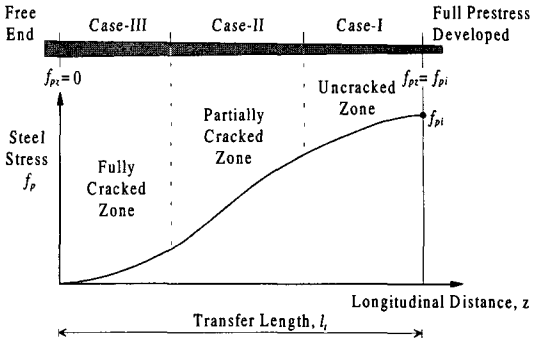

Fig. 11 Stress build-up in the transfer zone

Table 1 Comparison of theoretical and experimental results

Specimen Series*	f_{ci} (MPa)	f_{ck} (MPa)	f_{pi} (MPa)	Measured L_t (cm)		Calculated L_t (cm)
				Dead End	Live End	
S12-N-C3-1&2	33.6	47.9	1402.1	85.1	71.2	73.9
S12-N-C4-1&2	35.0	49.6	1391.9	66.9	56.9	59.6
S12-N-C5-1&2	33.6	47.9	1402.7	58.9	52.0	57.4
S12-H-C3-1&2	44.7	58.7	1359.3	69.2	58.0	65.3
S12-H-C4-1&2	46.3	59.1	1375.1	56.8	47.8	52.4
S12-H-C5-1&2	44.7	58.7	1394.7	51.3	45.9	51.6
S15-N-C3-1&2	35.0	49.6	1377.1	108.4	92.9	95.5
S15-N-C4-1&2	33.6	47.9	1392.5	83.9	74.8	70.3
S15-N-C5-1&2	35.0	49.6	1393.2	69.8	63.2	62.4
S15-H-C3-1&2	46.4	59.1	1357.5	88.8	76.2	85.4
S15-H-C4-1&2	44.7	58.7	1364.9	72.2	62.8	64.5
S15-H-C5-1&2	45.6	59.1	1384.4	57.4	51.3	56.7

* **S12** : nominal diameter of seven wire strand = 12.7mm,
S15: nominal diameter of seven wire strand = 15.2mm,
N : target strength at release = 35MPa, **H** : target strength at release = 45MPa,
C3, C4, C5 : clear bottom cover = 30, 40, 50 mm

8. Comparison of Theoretical Results with Test Data

In order to show the validity of proposed theoretical analysis, theoretical results were compared with some test data of author's experimental program.[16,17]

This program included an experimental investigation of transfer length of prestressing strands in pretensioned concrete beams. The major test variables include the nominal diameter of prestressing strands, concrete compressive strength, and bottom cover size. Twenty-four beams were made for transfer length tests Fig. 12. Each beam is identified by a numbering system to help identify the characteristics of that beam.

The theoretical transfer lengths in Table 1 are computed based on measured concrete strength at stress transfer (f_{ci}), initial prestressing level (f_{pi}), effective prestress and strand diameter. The theoretical and experimental strain curves for the beam S15-N-C3-1 are compared in Fig. 13. Except for the value of maximum strain, it can be seen that curves match well.

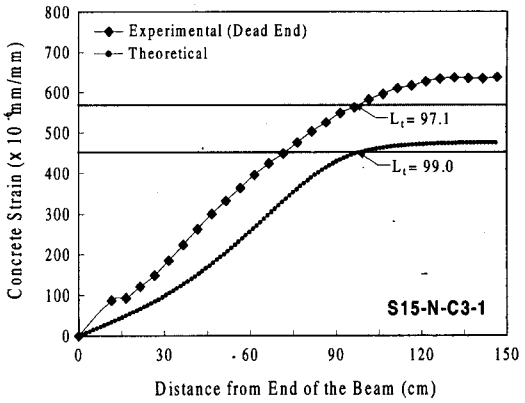

Fig. 13 Comparison of theoretical and experimental strain build-up curves for beam S15-N-C3-1

At the ends of the beams, measured concrete strains have increased due to combined effect of creep and shrinkage of the concrete. The difference between measured and calculated concrete surface strains is mainly due to these creep and shrinkage effect in the first 4 to 6 hours after release, while the measurements were being made.

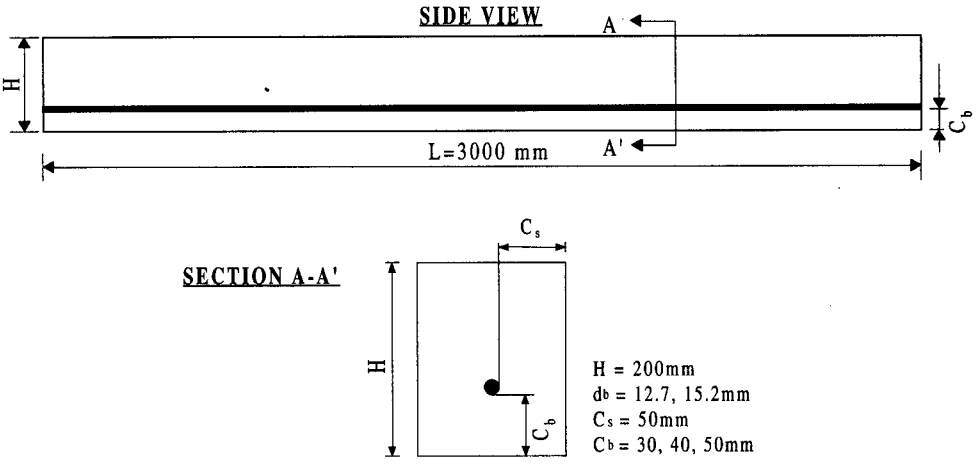

Fig. 12 Details of test beams

The theoretical and experimental transfer lengths are compared in Fig. 14 according to nominal strand diameter. The experimental transfer lengths are divided into two groups: "cut" end & "dead" end. The designations "cut" and "dead" are used for convenience to denote separate ends of the same specimen. The "cut end" refers to the end of the specimen where the strands are cut. The "dead end" is the end that releases stresses because of the cutting of the opposite side.

The differences between theoretical and experimental results are larger in the series with smaller cover. It can be seen from these figures that the trend of data match extremely well. Theoretical results lie between the value of dead end and cut end for almost every series. On average theoretical transfer lengths were larger than transfer lengths on dead end by 4.0% and smaller than transfer lengths on cut end by 9.7%.

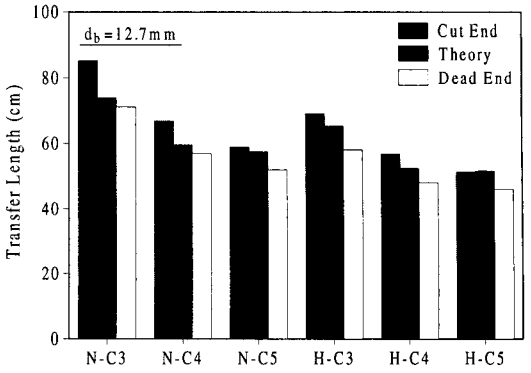

(a) Strand Diameter d_b = 12.7mm

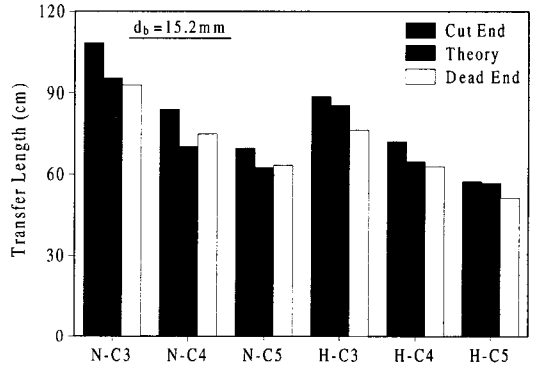

(b) Strand Diameter d_b = 15.2mm

Fig. 14 Comparison of theoretical and experimental transfer length

9. Conclusions

Based on the theoretical analysis and experimental investigation of this study the following conclusions can be drawn.

1. The analytical procedure presented in this paper successfully describes the stress and strain state in the transfer region. The effect of changes to one or more of the variables can therefore be predicted.
2. An elastic analysis of uncracked concrete surrounding a steel tendon in the outer part of the transfer zone will show tensile stresses which far exceed the concrete tensile strength. This indicates that radial crackings are expected to occur in this region.
3. The concrete in the transfer zone can be cracked to the surface, partially cracked, or uncracked depending on the tendon stress and size, concrete strength, and cover.
4. Transfer length increases with reduced cover and concrete strength. This trend of transfer length data calculated from the presented theory match well with experimental results.
5. The shape of the concrete strain profiles varies throughout the transfer zone ranging from concave, to linear, to convex in the prime portion of the transfer length.
6. The proposed analytical procedure in this study can be utilized as a useful tool for realistic evaluation of the transfer length in pretensioned, prestressed concrete member.

NOTATIONS

A	:	area of concrete section
A_p	:	area of prestressing steel
c_s	:	lower value of c_x and c_y
E_{cr}	:	Reduced circumferential modulus of elasticity at the outer surface of cracked concrete
e	:	outer radius of cracked zone
e_y	:	Eccentricity of prestressing steel
f_{cz}	:	axial stress in the concrete at a distance z from the free end
f_{pz}	:	axial stress in the prestressing steel at a distance z from free end
f_r	:	stress in radial direction
f_t	:	tensile strength of concrete
f_{tr}	:	Reduced tensile strength of concrete at the outer surface
I	:	second moment of area about the section centroid
L	:	gauge length
L_t	:	Transfer length
N	:	Number of radial cracks
R	:	radial distance to the inner boundary of uncracked section
w	:	crack width of radial cracks
y	:	Vertical distance to prestressing steel from section centroid
ν_c	:	Poisson's ratio for concrete
ν_p	:	Poisson's ratio for prestressing steel

References

1. Hoyer, E., and Friedrich, E., "Beitrag zür Frage der Hafspaannung in Eisenbeton-bauteilen," *Beton und Eisen*, Berlin, 1939, V. 30, No. 6, pp. 107-110.
2. Janney, J. R., "Nature of Bond in Pretensioned Prestressed Concrete," *ACI Journal*, Vol. 50, No. 9, May 1954, pp. 717–736.
3. Dinsmore, G. A., Deutsch, P. L., and Montemayor, J. L., *Anchorage and Bond in Pretensioned Prestressed Concrete Members*, Fritz Laboratory Report 223-19, Fritz Engineering Laboratory, Lehigh University, Bethlehem, Pennsylvania, December 1958, 188 pp.
4. Marshall, G., "End Anchorage and Bond Stress in Prestressed Concrete," *Magazine of Concrete Research*, Vol. 1, December 1949, pp. 123-127.
5. Guyon, Y., *Prestressed Concrete*, Contractors Record and Municipal Engineering, London, 1953.
6. Evans, R. H., and Robinson, G. W., "Bond Stress in Prestressed Concrete from X-ray Photographs," *Journal of the Institution of Civil Engineers*, Vol. 14, March 1955, Part 1, pp. 212-235.
7. Marshall, W. T., and Krishnamurthy, O., "Transmission Length of Prestressing Tendons from Concrete Cube Strengths at Transfer," *The Indian Concrete Journal*, Vol. 43, July 1969, pp. 244–253 and 257.
8. Tepfers, R., "Cracking of Concrete Cover along Anchored Deformed Reinforcing Bars," *Magazine of Concrete Research*, Vol. 31, No. 106, March 1979, pp. 3–12.
9. Laldji, S., and Young A. G., "Bond between Steel Strand and Cement Grout in Ground Anchorages," *Magazine of Concrete Research*, Vol. 40, No. 143, June 1988, pp. 90-98.
10. Ugural, A. C., and Fenster, S. K., *Advanced Strength and Applied Elasticity*, 3rd Edition, Prentice Hall, Upper Saddle River, NJ, 1995.
11. Weerasekera, I. R. A., *Transfer and Flexural Bond in Pretensioned Prestressed Concrete*, Ph.D. Dissertation, University of Calgary, Canada, June 1991.
12. Hillerborg, A., "Analysis of One Single Crack," *Fracture Mechanics of Concrete*, Developments in Civil Engineering, 7th Ed. Wittmann, F. H., Elsevier Science Publishers, Amsterdam, The Netherlands, 1983, pp. 223-249.
13. Shah, S. P., Swartz, S. E., and Ouyang, C., *Fracture Mechanics of Concrete,* John Wiley & Sons, New York, NY, 1995.
14. Gopalaratnam, V. S., and Shah, S. P., "Softening Response of Plain Concrete in Direct Tension," *ACI Journal*, Vol. 82, No. 3, May-June 1985, pp. 310–323.
15. Maron, M. J., and Lopez, R. J., *Numerical Analysis: A Practical Approach*, 3rd Edition, Wadsworth Publishing Company, Belmont, CA, 1991.
16. Oh. B. H. and Kim. E. S., "Realistic Evaluation of Transfer Lengths in Pretensioned Prestressed Concrete Members," in print, *ACI Structural Journal.*
17. Kim. E. S., *Analysis of Prestress Transfer Zone and Prediction of Transfer Length in Pretensioned Prestressed Concrete Member*, Ph.D Dissertation, Seoul National University, Korea, 2000.